Original paper

Krupičkaite, Cu$_6$[AsO$_3$(OH)]$_6$·8H$_2$O, a new copper arsenate mineral from Jáchymov (Czech Republic)

Gwladys STECIUK*[1], Jiří SEJKORA[2], Jiří ČEJKA[2], Jakub PLÁŠIL[1], Jan HLOUŠEK[3,†]

[1] *Institute of Physics, Academy of Sciences of the Czech Republic v.v.i, Na Slovance 2, 182 21 Prague 8, Czech Republic; steciuk@fzu.cz*

[2] *Department of Mineralogy and Petrology, National Museum, Cirkusová 1740, 193 00 Prague 9, Czech Republic*

[3] *Jáchymov, Czech Republic;*

[†] *deceased*

[*] *Corresponding author*

Krupičkaite, ideally Cu$_6$[AsO$_3$(OH)]$_6$·8H$_2$O, is a new supergene mineral from the Rovnost I shaft in Jáchymov, Czech Republic. It forms aggregates of pale greenish-blue color and grows along with supergene minerals crystallizing on the strongly altered relics of massive tennantite, Bi-rich tennantite, galena, chalcopyrite, bornite, and chalcocite with disseminated uraninite in quartz. For a long time, krupičkaite has been left out due to its quite inconspicuous appearance that can be mistakenly referred to as geminite. At the ambient temperature, krupičkaite is monoclinic, a = 15.504(7) Å, b = 18.144(7) Å, c = 10.563(5) Å, β = 103.30(4)°, V = 2891.5(2) Å^3, Z = 4, space group $P2_1/m$. Its structure has been solved and refined from 3D electron diffraction and further studied by Raman spectroscopy. The layered structure is built upon the alternation of two different copper-arsenate sheets stacked along b presenting a characteristic wave shape along the a–axis and separated by a thick interlayer with channels containing only H$_2$O. The collapsed chains of copper polyhedra are connected the same way as in geminite through AsO$_4$ tetrahedra. Krupičkaite joins the family of copper arsenate minerals with which it shares structural similarities at the level of the As-Cu layers with the lindackerite supergroup, slavkovite, or yvonite.

Keywords: krupičkaite, copper arsenate, crystal structure, electron diffraction, acid-mine-drainage, supergene weathering
Received: 4 November 2020; accepted: 10 March 2021; handling editor: F. Laufek
The online version of this article (doi: 10.3190/jgeosci.318) contains supplementary electronic material.

1. Introduction

Under oxidizing conditions, decomposition of hypogene/primary As-containing sulfides and sulfosalts potentially leads to a release into the environment of significant amounts of arsenic, heavy metals and metalloids. In ore deposits, supergene minerals are formed as resulting products of these reactions and they serve as a temporary or final sink for such toxic elements otherwise released into the groundwater systems. The danger associated with arsenic in the environment, combined with its unusually great mineralogical diversity poses a set of specific challenges to mineralogy and environmental geochemistry (Majzlan et al. 2014; Christy 2015). To give proper answers and solutions to the environmental problems, the detailed knowledge of mineralogy, crystallography, physical and chemical properties of As-containing oxysalts are of great importance as it can be used to assess and predict the behavior and the mobility of elements during weathering, both natural or anthropogenically induced (e.g., Borčinová Radková et al. 2017; Keim et al. 2018; Majzlan et al. 2018, 2021; Đorđević et al. 2019, and references therein).

Krupičkaite, ideally Cu$_6$[AsO$_3$(OH)]$_6$·8H$_2$O, is a new copper arsenate hydrate found from the strongly weathered material originating from the famous Rovnost I shaft in Jáchymov, Czech Republic. It has been formed *via* oxidative weathering of a complex hypogene mineral association (including namely tennantite and Bi-rich tennantite) at the Geister vein. Although it is currently known only from a few specimens, it is likely to be much more common and overlooked due to its relatively inconspicuous appearance that can be mistakenly referred to as geminite.

The new mineral honors the name of professor Jiří "George" Krupička (born in Prague, Czech Republic, May 5, 1913; died in Edmonton, Canada, April 24, 2014), first of all, a polymath; linguist, geologist and astronomer by education.

The new mineral was approved by the CNMNC IMA under the code IMA 2020–032. The holotype specimen of krupičkaite is deposited in the collections of the Department of Mineralogy and Petrology, National Museum in Prague, Cirkusová 1740, 19300 Praha 9, Czech Republic under the catalogue number P1P 18/2020. The aim of this work is to document the physical and chemical attributes of the new species, and to shed light on its crystal structure.

2. Occurrence

Krupičkaite was found in 1978, in an old ore-stope near-surface workings at the 3rd Geister level of the Rovnost I (former Werner) mine. Rovnost I mine, in Jáchymov (Czech Republic), opened and remained the main shaft of the so-called Western district of Jáchymov mines, situated at the center of the Rovnost ore node. This stope was reopened during the first half of the 19th century and later on in the 1950ties. The main aim was mining for Ra and U, used for glass-staining in the 19th century and later implementing the Soviet atomic arsenal. The more detailed information about history, geology and mineralogy of this particular locality can be found elsewhere (Ondruš et al. 2003; Hloušek et al. 2014; Horák et al. 2014; Plášil et al. 2017; Škácha et al. 2019). The mineral richness of the locality results from the occurrence of both the recently/sub-recently formed minerals connected with the post-mining processes, and the supergene minerals formed *in-situ* in the oxidation zone (association of uranyl arsenates and vanadates; association of Pb-Cu supergene minerals and minerals containing Y and *REE*). The shaft where krupičkaite was found is informally called the "lindackerite stope" by mineral collectors. This name is due to frequent occurrences of the lindackerite-supergroup minerals: lindackerite, veselovskýite (Sejkora et al. 2010a), hloušekite (Plášil et al. 2014a), pradetite (unpublished data of the authors) and klajite (Plášil et al. 2014b; Hloušek et al. 2014). A copper-dominant vivianite-group mineral, babánekite (Plášil et al. 2017), has been found from the same material as krupičkaite.

Supergene minerals crystallize on the strongly altered relics of massive tennantite, Bi-rich tennantite, galena, chalcopyrite, bornite, and chalcocite with disseminated uraninite in quartz (in the absence of carbonates). Krupičkaite grows along with those above-mentioned minerals, forming rather inconspicuous aggregates of pale greenish-blue color. The richest specimens were found in the intensively cemented fragments with relics of primary minerals.

3. Appearance and physical properties

Krupičkaite appears in rounded or grape-like aggregates composed of hundreds of microcrystals that are not larger than the first microns. These aggregates have greenish-blue color, occasionally with a grey tint, and reach up to 4 mm in size, sitting at the surface of the supergene crusts (Fig. 1). Krupičkaite has a vitreous luster. The streak is white. The Mohs hardness is estimated at 2 (based on scratch tests). No cleavage nor tenacity has been observed. The mineral is not fluorescent under long- or short-wave ultraviolet radiation. A density of 3.123 g/cm^3 was calculated using the empirical formula and unit-cell parameters obtained from powder X-ray diffraction. Direct density measurements were not undertaken due to the paucity of pure material. Optical properties could not have been determined due to the extremely small size of the crystals; the mean *n* calculated from Gladstone–Dale rule is 1.597 (empirical formula) or 1.5975 (ideal formula).

4. Chemical composition

Chemical analyses of krupičkaite were carried out with a Cameca SX 100 electron microprobe (WDS mode, 15 kV, 5 nA, 20 μm defocused beam diameter). Analytical lines and standards are given in Tab. 1; peak counting times were 10–20 s and the counting time for the background their half. The measured intensities were processed for matrix effects using the "*PAP*" correction routine (Pouchou and Pichoir 1985). Water could not be analyzed directly because of the small amount of pure material available and was calculated on the basis of 8 H_2O from the structure analysis. Results (average of 22 analyses) are given in Tab. 1. After the inclusion of water content, the higher analytical total indicates partial dehydration of the sample under vacuum in the EPMA chamber.

The empirical formula of the aggregate of krupičkaite, on the basis of 32 anions *apfu*, is $(Cu_{5.16} Co_{0.34} Ni_{0.33} Zn_{0.11} Ca_{0.05} Fe_{0.01} Mn_{0.01})_{\Sigma6.01}(AsO_3OH)_{5.97}(SiO_4)_{0.03} (PO_3OH)_{0.01} \cdot 8H_2O$. The ideal formula $Cu_6[AsO_3(OH)]_6 \cdot 8H_2O$ requires CuO 34.97, As_2O_5 50.51, H_2O 14.52, total 100.00 wt. %. Krupičkaite is visibly

Tab. 1 Analytical data (wt. %) for krupičkaite

Constituent	Mean	Range	Standard deviation	Probe Standard
CuO	31.83	29.35–33.12	0.95	chalcopyrite
CaO	0.22	0.08–0.50	0.11	fluorapatite
CoO	1.95	1.62–2.58	0.25	Co
NiO	1.90	1.45–2.71	0.34	Ni
MnO	0.05	0–0.23	0.06	rhodonite
ZnO	0.68	0.43–0.87	0.11	ZnO
FeO	0.06	0–0.17	0.05	hematite
SiO$_2$	0.14	0–0.44	0.13	sanidine
As$_2$O$_5$	53.16	50.86–54.75	1.04	clinoclase
P$_2$O$_5$	0.06	0–0.31	0.09	fluorapatite
H$_2$O*	15.35			
Total	105.40			

* Content of H_2O was calculated on the basis of ideal composition derived from results of the crystal structure study
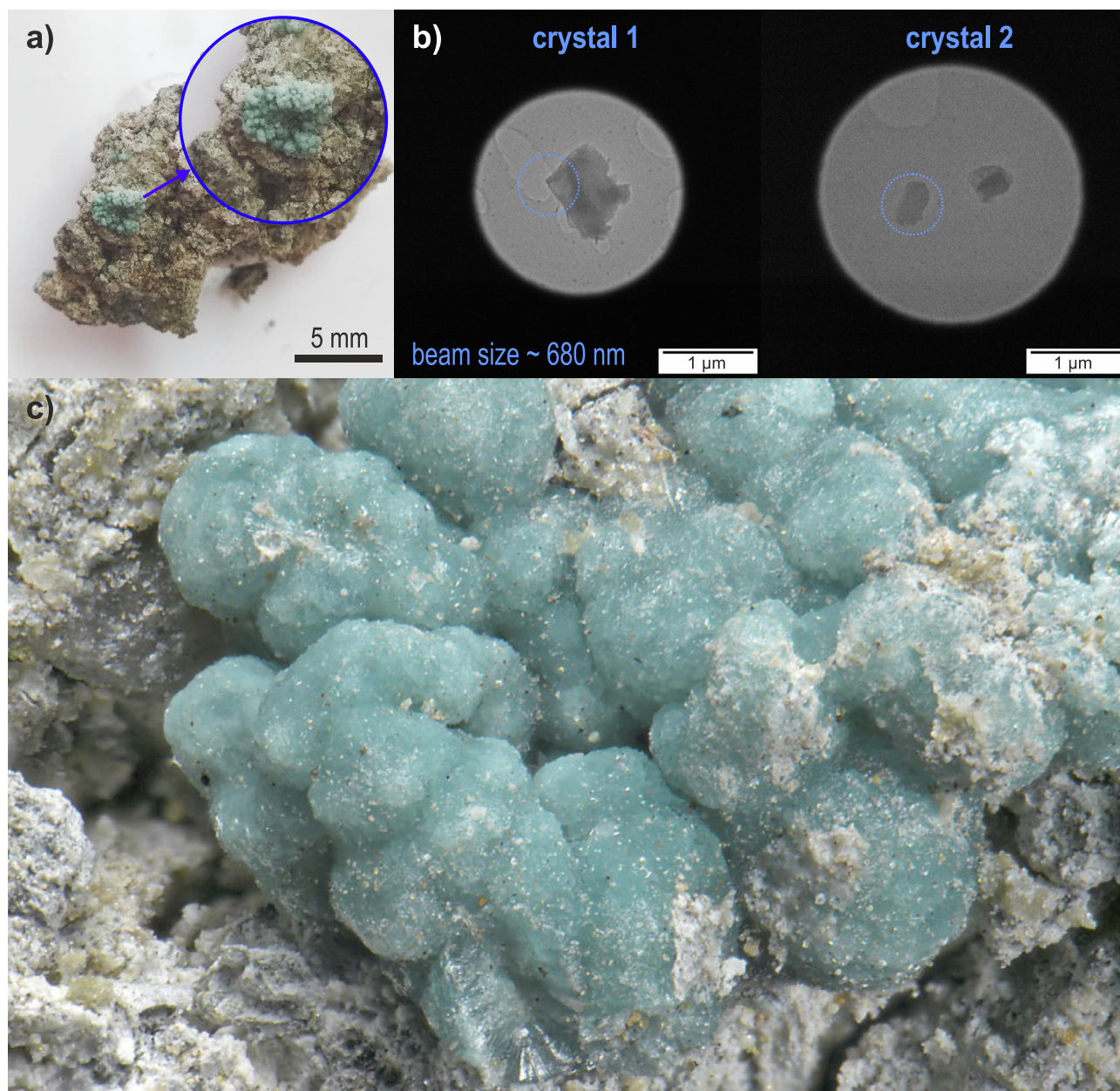
Fig. 1 a) Krupičkaite aggregates on gangue used for the crystallographic analysis. **b)** Two krupičkaite crystals selected for 3D ED data acquisition collected on the sample shown in a). **c)** Light greenish–blue hemispherical aggregates of krupičkaite on strongly supergene altered gangue, Jáchymov; holotype specimen, width of the photograph is 3.7 mm, photo J. Sejkora.

insoluble in H_2O and soluble in dilute (10 %) HCl, at room temperature.

5. Raman spectroscopy

The Raman spectrum (Fig. 2) was collected in the range 4000–50 cm^{-1} using a DXR dispersive Raman Spectrometer (Thermo Scientific) mounted on a confocal Olympus microscope. The Raman signal was excited by an unpolarised red 633 nm He-Ne gas laser and detected by a CCD detector. The experimental parameters were: 100× objective, 10 s exposure time, 100 exposures, 400 lines/mm grating, 50 μm pinhole spectrograph aperture and 5 mW laser power level. The instrument was set up by a software-controlled calibration procedure using multiple neon emission lines (wavelength calibration), multiple polystyrene Raman bands (laser frequency calibration) and standardized white-light sources (intensity calibration). Spectral manipulations were performed using the Omnic 9 software (Thermo Scientific). The main bands observed
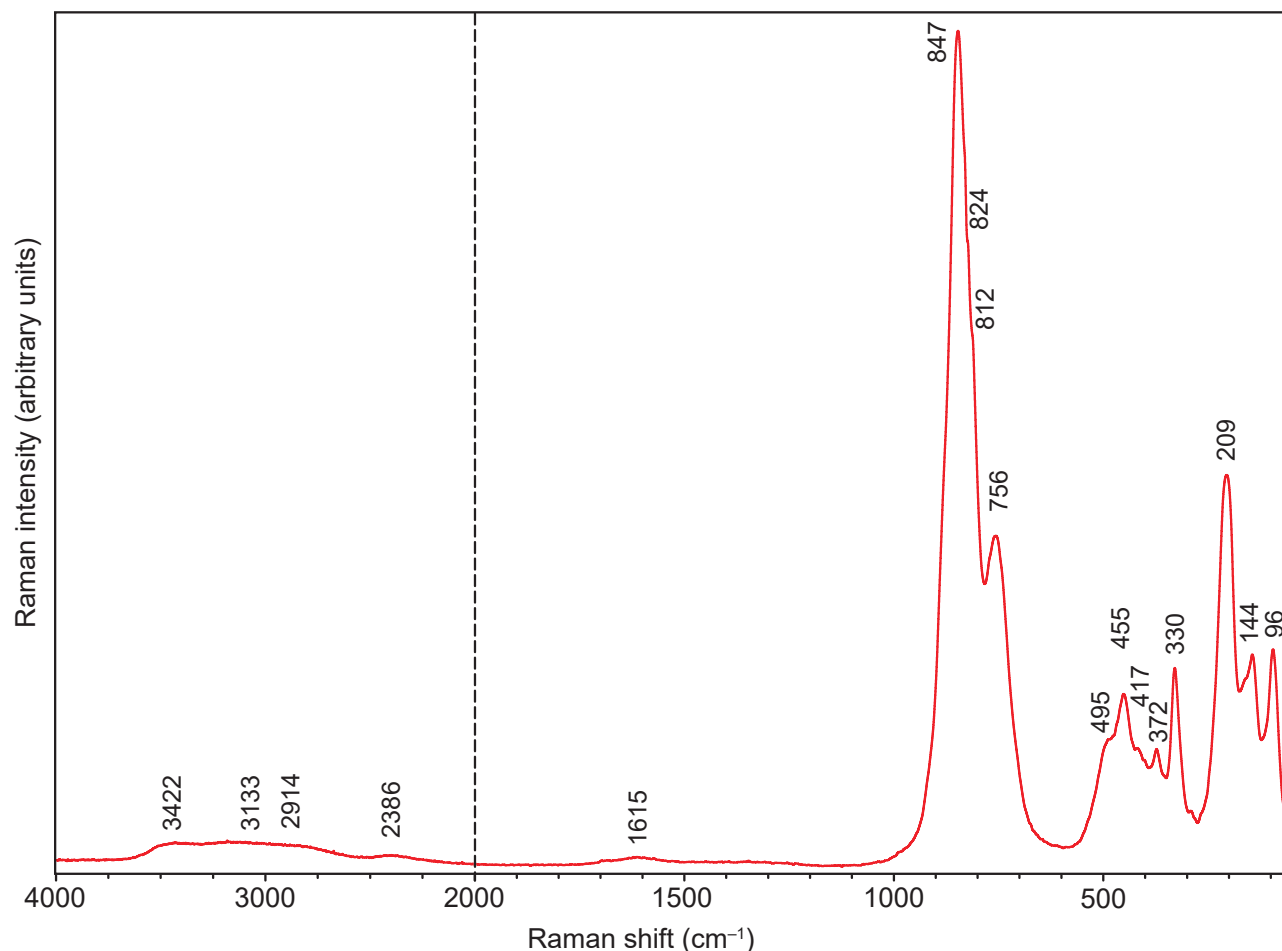
Fig. 2 Raman spectrum of krupičkaite from Jáchymov (split at 2000 cm⁻¹).

are (in wavenumbers): 3422, 3133, 2914, 2386, 1615, 847, 824, 812, 756, 495, 455, 417, 399, 372, 330, 209, 144 and 96 cm⁻¹. Very weak broad Raman bands with topics at 3422 and 3133 cm⁻¹ are assigned to the ν OH stretching vibrations of structurally distinct differently hydrogen-bonded water molecules. Very weak broad Raman bands with topics at 2914 and 2386 cm⁻¹ are connected with ν OH stretching vibrations in hydrogen-bonded $(AsO_3OH)^{2-}$ units. A very weak broad Raman band at 1615 is assigned to the ν_2 (δ) H_2O bending vibrations of water molecules. The most prominent very strong Raman bands at 847 and 756 cm⁻¹ with shoulders at 824 and 812 cm⁻¹ are attributed to overlapping ν_1 $(AsO_3OH)^{2-}$ symmetric stretching, and ν_3 $(AsO_3OH)^{2-}$ antisymmetric stretching vibrations. Raman bands 495, 455, 417 and 399 cm⁻¹ are connected with the ν_4 $(HOAsO_3)^{2-}$ bending vibrations. Raman bands at 372 and 330 cm⁻¹ are related to the ν_2 (δ) $(HOAsO_3)^{2-}$ bending vibrations. Raman band at 209 cm⁻¹ is assigned to the ν (OH···O) stretching vibrations and those at 144 and 96 cm⁻¹ to lattice modes (Vansant et al. 1973; Čejka et al. 2011; Sejkora et al. 2010b, 2020).

6. Crystallography

6.1. Powder X–ray diffraction

X–ray powder diffraction data of krupičkaite (Tab. 2) were recorded at room temperature using a Bruker D8 Advance diffractometer equipped with a solid-state Lynx-Eye detector and secondary monochromator producing CuK_α radiation housed at the Department of Mineralogy and Petrology, National Museum, Prague, Czech Republic. The instrument was operating at 40 kV and 40 mA. To minimize the background, the powder samples were placed on the surface of a flat silicon wafer. The powder pattern was collected in the Bragg–Brentano geometry in the range 3–70° 2θ, step 0.01° and counting time of 20 s per step (total duration of the experiment was ca. 30 hours). The positions and intensities of diffractions were found and refined using the Pearson VII shape function of the ZDS program package (Ondruš 1993). The unit-cell parameters were refined (starting from those obtained by the electron diffraction) by the least-squares program of Burnham (1962) as follows: *a* = 15.504(7) Å, *b* =

18.144(7) Å, c = 10.563(5) Å, β = 103.30(4)° and V = 2891.5(2) Å³.

6.2. Electron diffraction

Due to the nature of the crystals (powdery, indistinct morphology even under scanning electron microscope), transmission electron microscopy (TEM) has been chosen to investigate the structural properties of krupičkaite. Aggregates of the new mineral were gently crushed without solvent and deposited on an Au-grid with a thin film of holey amorphous carbon. The grid was plunged into liquid nitrogen and then transferred to a FEI Tecnai TEM (acceleration voltage of 200 kV, LaB$_6$) using a Gatan cryo-transfer holder. The cryo-plunging conditions were necessary to preserve the hydrated nature of krupičkaite under the TEM vacuum. Without this precaution, our TEM experiments showed that krupičkaite undergoes fast dehydration inducing a drastic change in the layer configuration. This is also associated with very strong diffuse features in the data that

Tab. 2 Powder diffraction data (d in Å) for krupičkaite

$I_{obs.}$	$d_{obs.}$	$d_{calc.}$	h	k	l	$I_{obs.}$	$d_{obs.}$	$d_{calc.}$	h	k	l
0.13	11.6221	11.6007	1	1	0	0.23	2.7325	2.7340	0	4	3
100.00	**9.0895**	9.0719	0	2	0	0.16	2.7206	2.7224	4	1	2
0.03	5.4809	5.4839	2	2	−1	0.03	2.6510	2.6507	2	6	1
0.22	4.8096	4.8148	3	1	−1	0.23	2.6191	2.6151	4	5	0
0.07	4.7440	4.7585	1	3	1	0.11	2.6058	2.6063	0	6	2
0.07	4.5457	4.5424	1	2	−2	0.18	2.5186	2.5194	1	6	2
0.07	4.5341	4.5360	0	4	0	0.03	2.5126	2.5126	3	1	−4
0.48	4.3945	4.3985	3	2	0	0.07	2.4902	2.4913	0	5	3
0.13	4.0070	3.9959	3	1	−2	0.15	2.4128	2.4074	6	2	−2
0.51	**3.9094**	3.9095	1	4	1	0.06	2.3904	2.3957	4	0	−4
0.30	3.8448	3.8508	3	3	−1	0.17	2.3557	2.3545	5	5	−1
0.13	3.7344	3.7335	3	2	−2	0.20	2.3031	2.3006	3	7	−1
0.06	3.6871	3.6929	4	1	0	0.21	2.2113	2.2143	7	0	−1
1.03	**3.5334**	3.5348	4	2	−1	0.19	2.1986	2.1993	3	7	1
0.47	3.3687	3.3683	3	4	0	0.11	2.1573	2.1512	7	2	−1
		3.3669	0	1	3	0.07	2.1344	2.1316	2	3	4
0.25	3.2819	3.2823	1	2	−3	0.11	2.0431	2.0459	7	3	−2
0.42	3.2441	3.2407	4	3	−1	0.01	1.9973	1.9980	5	4	−4
0.06	3.1865	3.1867	1	0	3	0.25	1.9818	1.9869	5	5	2
0.32	3.1078	3.1043	4	2	1	0.10	1.9537	1.9561	6	5	1
0.36	3.0852	3.0942	5	0	−1	0.17	1.8147	1.8138	3	9	1
0.18	3.0296	3.0240	0	6	0	0.22	1.7832	1.7838	4	8	−3
0.13	2.9781	2.9846	1	5	−2	0.02	1.7575	1.7566	6	3	3
0.93	**2.9724**	2.9812	0	3	3	0.01	1.7501	1.7509	5	7	2
0.54	**2.9372**	2.9356	3	5	−1	0.10	1.7452	1.7446	5	8	1
0.26	2.9286	2.9300	4	4	−1	0.09	1.7066	1.7056	0	1	6
0.17	2.8877	2.8838	1	6	−1	0.15	1.6842	1.6856	1	10	2
0.22	2.8399	2.8384	1	5	2	0.09	1.6803	1.6799	6	4	−5
0.08	2.7887	2.7813	1	4	−3						
0.33	2.7595	2.7546	5	3	−1						
		2.7536	4	0	2						

hamper a reliable structural analysis. The cryo-plunging method, initially used for organic and biological samples, was recently applied to inorganic samples (Mugnaioli et al. 2020; Steciuk et al. 2020; Steciuk et al. 2021). To collect 3D electron diffraction (3D ED) data on single crystals (Gemmi and Lanza 2019), the precession electron diffraction tomography (PEDT) technique was used (Vincent and Midgley 1994; Kolb et al. 2007, 2008; Mugnaioli et al. 2009). In order to reduce dynamic effects, 3D ED was coupled with precession electron diffraction (PED) (Vincent and Midgley 1994). PEDT data were recorded at 100 K on several crystals with the precession device Nanomegas Digistar and a side-mounted CCD camera Olympus Veleta with a 14bit dynamic range and an energy-dispersive analyzer Octane silicon drift detector (SDD) EDAX. The precession angle of the beam was kept at 1°. For each selected crystal, a series of non–oriented patterns are collected sequentially on all the accessible tilt–range of the goniometer by step of 1°. For more details about the data acquisition, see Palatinus et al. (2015b) or Gemmi et al. (2019). Low illumination settings were used to preserve

the crystals under the electron beam during the experiment. The data reduction was performed using the computer programs PETS2.0 (Palatinus et al. 2019). Based on two merged data sets, krupičkaite is monoclinic, with a = 15.25 Å, b = 17.59 Å, c = 10.27 Å, β = 103.42°, and V = 2681.6 Å³ (Fig. 3a). No phase transition is observed between krupičkaite measured from 3D ED at 100K and at the ambient temperature (PXRD). The reciprocal space sections are consistent with the space group $P2_1/n$ (with the condition $h+l$ = 2n on $h0l$) (Fig. 3b). The experimental intensity profile (rocking curve) is fitted using several parameters, including the rocking curve width (RC width = 0.003 Å^{-1}) and the apparent mosaicity (mosaicity = 0.15°) (for detailed information, check Palatinus et al. 2019). The high value of the apparent mosaicity is mostly due to stacking faults resulting in elongated reflections along b* (default values in PETS2.0: RC width = 0.001 Å^{-1} and apparent mosaicity = 0.05°). For each PEDT data set, two hkl-type files are obtained: one for structure solution and kinematical refinement and another file dedicated to the dynamical refinement where each ED frame is considered

Tab. 3 Summary of data collection conditions and refinement parameters for krupičkaite

Refined structural formula	$Cu_6(H_2O)_6[AsO_3(OH)]_6(H_2O)_{2.216}$
Unit-cell parameters (PEDT) 100K	
a	15.25 Å
b	17.59 Å
c	10.27 Å
$\alpha = \gamma$	90°
β	103.42°
V	2681.6 Å³
Z	4
Density [g·cm⁻³]	3.3794
Space group	$P2_1/n$
Temperature	100 K
TEM	FEI Tecnai 02
Radiation (wavelength)	electrons (0.0251 Å)
Resolution range $\sin\theta/\lambda$	0.1–0.7 Å⁻¹
Limiting Miller indices	$-21 \leq h \leq 20,\ 0 \leq k \leq 24,\ 0 \leq l \leq 14$
No. of independent reflections (obs/all) – kinematic	1803/7132
R_{int} (obs/all) – kinematic	crs1: 0.1345/0.6285 and crs2: 0.1652/0.3142
Redundancy	4.892
Coverage for $\sin\theta/\lambda = 0.7$Å⁻¹	0.91
Kinematical refinement with hydrogen	
No. of reflections (obs/all)	1803/7132
R, wR (obs)	0.2157/0.1785
N parameters	201
Dynamical refinement with hydrogen	
RSg(max) (crs1 and crs2)	0.6
No. of reflections (obs/all)	7089/38210
R, wR (obs)	0.1523/0.1457
N parameters/N struct. parameters	350/196
Crystal thickness (crs1, crs 2)	476(8) Å and 322(3) Å

independent (Palatinus et al. 2015a, b). The data completeness reached 91% for a $\sin\theta/\lambda = 0.7$ Å⁻¹ resolution shell after combining two data sets (Tab. 3). The structure was solved with Superflip (Palatinus and Chapuis 2007) and refined in Jana2006 (Petříček et al. 2014).

6.3. Structure solution and refinement

A complete structure solution was obtained with the Superflip program, and only the atomic types were adjusted according to the relevant cation-oxygen distances. Surprisingly and considering the limited data quality, the electrostatic potential map presents very well-defined peaks corresponding to the copper-arsenate layer. The cationic sites possessing cation-oxygen distances of about 1.7 and 2 Å are attributed to arsenate and copper polyhedra, respectively.

For the refinement of krupičkaite structure against 3D ED data, neither the kinematical refinement nor the dynamical refinement is able to account for the diffuse scattering visible along the stacking direction, and more generally, inelastic scattering is not modeled (see sections in Fig. 3b) (Latychevskaia and Abrahams 2019).

For krupičkaite, the elongated reflections did not prevent the structure solution. However, the accuracy of refinement is affected. If the dynamical refinement is the most accurate for well-crystallized crystals and can easily reach R-factors below 8–10 % (Palatinus et al. 2015b; Steciuk et al. 2019a), imperfect crystals tend to diffract more kinematically. In such a case, the question is then to evaluate if the use of the dynamical theory in the refinement brings further improvement compared to the refinement ignoring them (kinematical refinement), especially when the dynamical refinement takes weeks, as it is the case for krupičkaite. Several works already report similar issues in the analysis of 3D ED data by going from some diffuse phenomenon reducing the precision of the refinement (Steciuk et al. 2019b) to the impossibility of solving and or refining the structure from 3D ED data (Zhao et al. 2017; Krysiak et al. 2018). In the latter cases, a quantitative analysis of the disorder is necessary to fully understand the structure and the related properties (Brázda et al. 2016; Neagu and Tai 2017; Zhao et al. 2017; Krysiak et al. 2018; Mugnaioli and Gorelik 2019).

For 3D ED data collected on krupičkaite crystals, the R-values from the dynamical refinement are significantly lower than the kinematical ones and still reach reasonable values with $R(obs) = 0.1523$ and $wR(obs) = 0.1457$ for 7089 unique observed reflections (Tab. 3). Moreover, the dynamical refinement was more efficient in revealing hydrogen positions, despite some were already visible using the kinematical approximation (Steciuk et al. 2021). For these reasons, the structural description is based on the results of the dynamical refinement that is considered, in this case, slightly more accurate than the kinematical one in terms of positional parameters. The low data resolution and the disorder did not allow the refinement of the atomic displacement parameters with the dynamical refinement. They were set to the value obtained from the kinematical refinement where only two values were refined: one unique value for As and Cu atoms and one for all O atoms. Moreover, to ensure the coordination polyhedra's stability with reasonable cation-oxygen distances, restric-
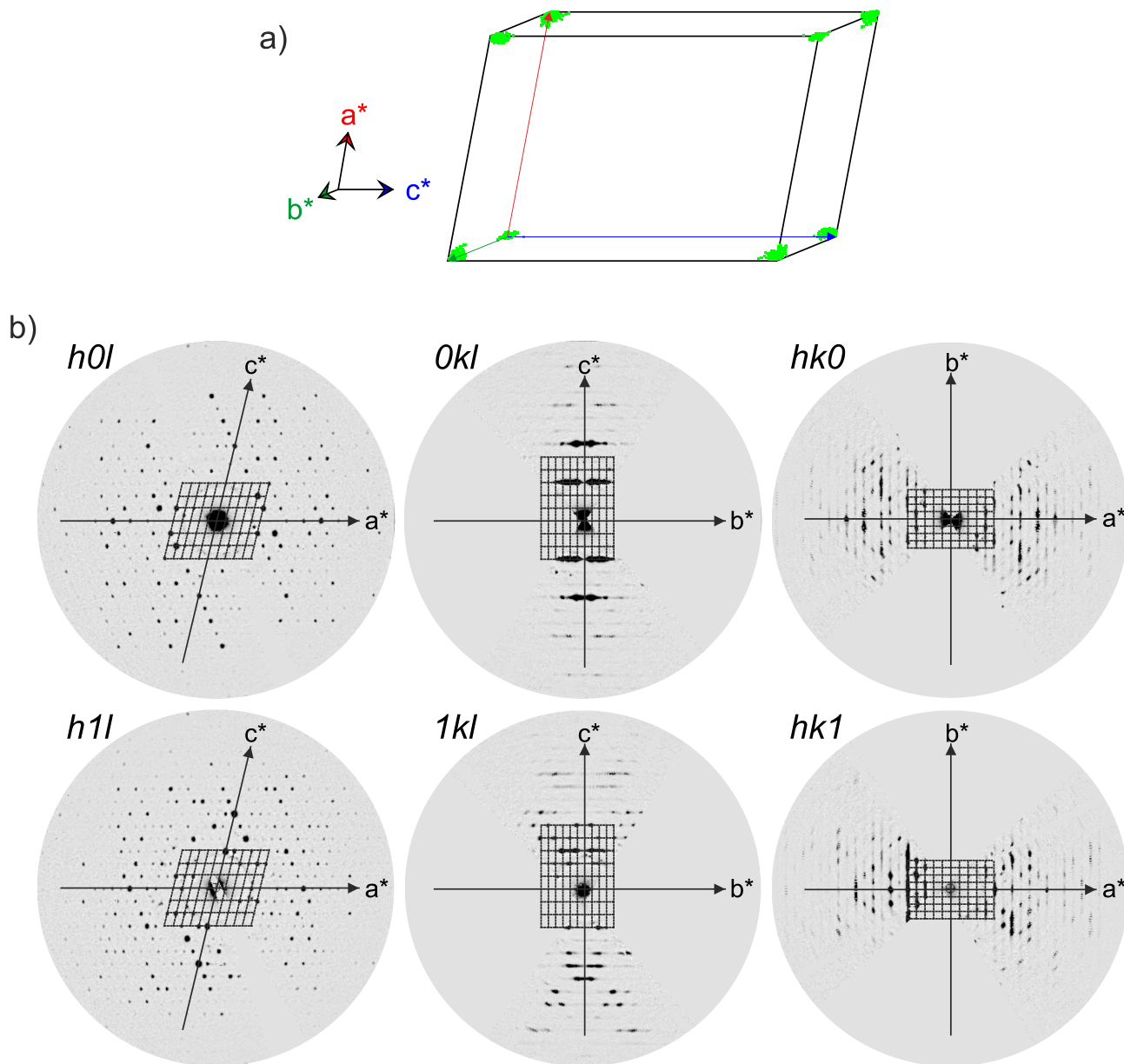
Fig. 3 Reciprocal–space reconstruction: **a)** Projected within one unit cell; **b)** sections of the reciprocal space from PEDT data.

tions were applied on As–O, Cu–O and O–O distances. The difference potential map allows the determination of 14 hydrogen positions of the 18 expected despite a very noisy map. The last ones (labelled H1O1, H1O6, H2O10, and H2O17) were deduced by geometry in order to stabilize them with a strong hydrogen bond as it has been observed in geminite (Cooper and Hawthorne 1995; Prencipe et al. 1996). While the apparent O–H distance is still an open question for electron diffraction data (Clabbers et al. 2019), our data are not suitable to test it and O–H distances were set to 0.98 Å with the isotropic displacement parameters of the hydrogen atoms set as riding with an extension factor of 1.2 (Palatinus et al. 2017).

From the refinement, the hydrogen positions of the inter-channel water molecules are not visible in the difference potential map because the corresponding oxygen sites are all partially occupied and most likely disordered. The refined water content is 2.216 for $Z = 4$. This value is probably a rough estimation since the atomic displacement parameters could not be refined. However, the experience shows that in the case of a disordered site, the refined occupancy is usually overestimated. Thus, the formula of krupičkaite for $Z = 4$ is probably close to $Cu_6(H_2O)_6[AsO_3(OH)]_6(H_2O)_2$. It means that from our 3D ED data collected under the TEM vacuum, only half of the H_2O sites intra-channel are occupied. Even though the cryo plunging method was used, we cannot exclude
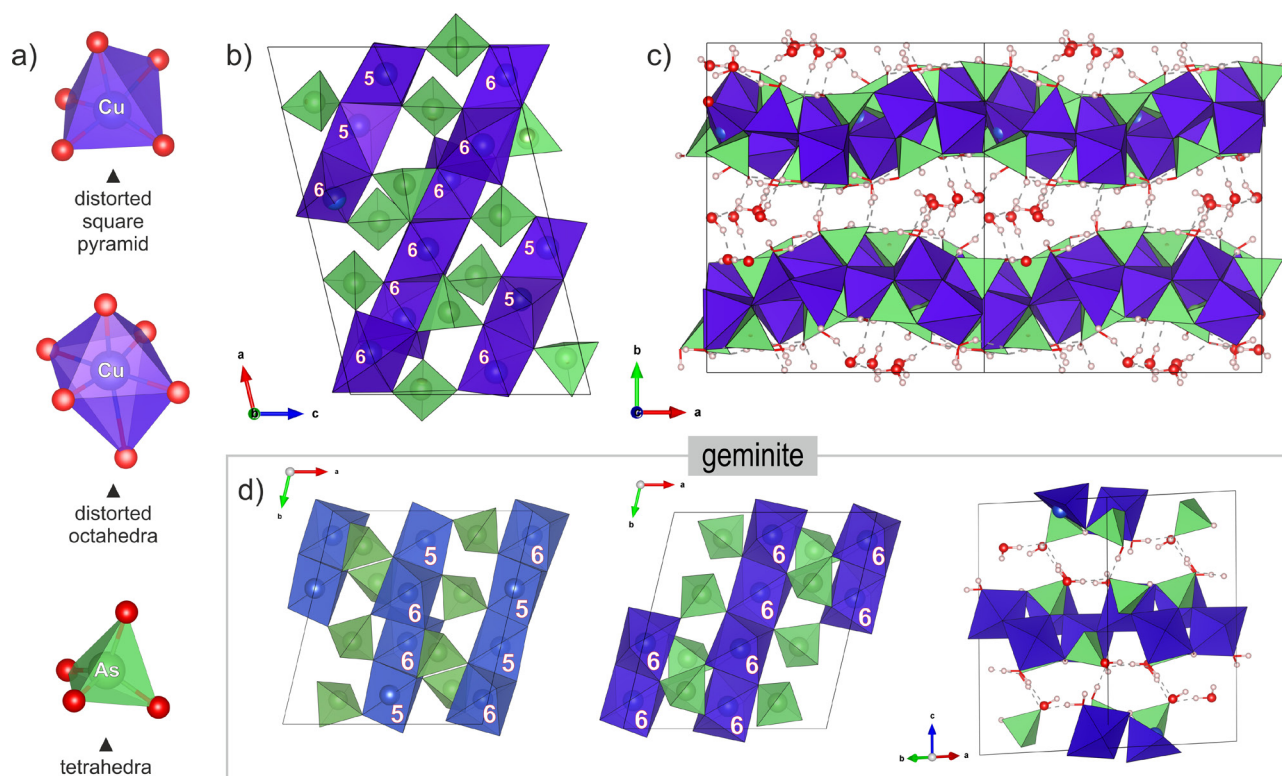
Fig. 4 a) Cation coordination polyhedra found in krupičkaite. **b)** Topology of the copper–arsenate layer. **c)** [001] projections of the structure showing the stacking sequence of krupičkaite Cu$_6$[AsO$_3$(OH)]$_6$·8H$_2$O. **d)** Topology and stacking in geminite Cu(AsO$_3$OH)·H$_2$O (after Cooper and Hawthorne 1995).

an influence of the TEM vacuum on the apparent amount of water. The CIF file, also containing a block with the reflections, is deposited at the Journal's webpage *www.jgeosci.org*.

7. Crystal structure

7.1. Cation coordination and connectivity

The structure of krupičkaite possesses six Cu, six As, thirty-four O (four of them belong to the water molecules not-bonded directly to any metal cation), and eighteen H sites when the hydrogen sites of the water in the channel is not considered (14 have been directly revealed by the current study) (Tab. 4). The copper sites were considered to be only occupied by Cu^{2+}, despite the fact that elevated contents of Ni and Co have been detected in the WDS data. Due to similar atomic-scattering amplitude for electrons for Cu, Ni and Co, the refinement from PEDT data of their respective occupancies was not possible. Hence, all positions are treated in the refinements as fully occupied by Cu. In terms of coordination polyhedral, Cu^{2+} occupies both distorted square pyramids [4+1], and distorted octahedra [4+2], while Cu1 site is in [4+2] coordination with four O^{2-} and two (H$_2$O) groups. Cu2 and Cu6 sites are also in [4+2] coordination but surrounded by five O^{2-}

and only one (H$_2$O) group. The Cu4 site is the only copper site in octahedral coordination that is not bonded to any water molecule because each of its vertices is connected to the vertex of an As-tetrahedra. The Cu3 and Cu5 sites are in [4+1] coordination with four O^{2-} and one (H$_2$O) group. The coordination polyhedra around Cu are all distorted due to the Jahn–Teller effect (Burns and Hawthorne 1995), inducing a wide range of Cu–O distances ranging from 1.769(11) to 2.376(5) Å (Tab. 5 and Fig. 4a). All As sites are in tetrahedral coordination and are occupied by pentavalent As ions. The average As–O distance of 1.68 Å was restricted during the refinement to stay within the range most-frequently exhibited by AsO$_4$ tetrahedra. In the same way, as for geminite, all As-groups are protonated, exhibiting three oxygen anions and one OH group for which the As–OH distance tends to be the longest As–O distance in each of the tetrahedra (Tab. 5).

As shown in Figs 4b and c, krupičkaite possesses an original topology with the copper-arsenate layer forming a wave shape along the **a**-axis, that is characteristic of this mineral. Within one layer, the structure of krupičkaite is built upon infinite chains of CuΦ$_5$ and CuΦ$_6$-polyhedra sharing edges to form infinite layers parallel to (010) and linked together by As-tetrahedra to form infinite sheets. There are two symmetrically distinct chains within one layer: one with only 6-coordinated Cu and another with a mixture of 5- and 6-coordinated

Tab. 4 Atom positions and displacement parameters (Å²) and bond–valence sums (BV, in valence–units) for krupičkaite as obtained from dynamical refinement

atom	x/a	y/b	z/c	Occ	BV[#]	U_{iso} *
As1	0.23482(13)	0.8246(3)	0.4930(2)	1	5.03(4)	0.0078(5)
As2	0.60343(14)	0.8189(3)	0.4325(2)	1	5.15(5)	0.0078(5)
As3	0.01903(14)	0.7152(3)	0.3008(2)	1	5.30(5)	0.0078(5)
As4	0.32106(14)	0.7841(2)	0.1261(2)	1	5.22(5)	0.0078(5)
As5	0.34173(14)	0.6283(2)	0.6385(2)	1	5.31(5)	0.0078(5)
As6	0.49637(14)	0.6214(2)	0.2899(2)	1	5.18(4)	0.0078(5)
Cu1	0.42094(19)	0.6619(3)	0.9650(3)	1	1.94(2)	0.0078(5)
Cu2	0.61934(16)	0.6851(3)	0.6260(2)	1	2.01(2)	0.0078(5)
Cu3	0.27092(15)	0.7633(3)	0.8018(2)	1	2.18 (2)	0.0078(5)
Cu4	0.41916(17)	0.7510(2)	0.4643(3)	1	2.23(2)	0.0078(5)
Cu5	0.56273(15)	0.7662(3)	0.1271(2)	1	2.19(2)	0.0078(5)
Cu6	0.21644(16)	0.6875(3)	0.2970(2)	1	2.02(2)	0.0078(5)
O1	0.6543(4)	0.9058(4)	0.4404(6)	1	2.15(4)	0.0142(7)
O2	0.3386(4)	0.5798(4)	0.9895(7)	1	2.29(5)	0.0142(7)
O3	0.5930(4)	0.8605(5)	0.0968(6)	1	2.46(5)	0.0142(7)
O4	0.1821(4)	0.7899(4)	0.3448(5)	1	2.00(2)	0.0142(7)
O5	0.1036(4)	0.6525(5)	0.3425(6)	1	1.87(3)	0.0142(7)
O6	0.1929(4)	0.9162(3)	0.4854(7)	1	2.09(4)	0.0142(7)
O7	0.2535(3)	0.5676(4)	0.6307(6)	1	2.22(6)	0.0142(7)
O8	0.4963(4)	0.6706(5)	0.1543(4)	1	2.18(3)	0.0142(7)
O9	0.5965(3)	0.5747(3)	0.6336(6)	1	2.14(6)	0.0142(7)
O10	0.2421(4)	0.5842(4)	0.2437(6)	1	2.25(5)	0.0142(7)
O11	0.6540(4)	0.7878(5)	0.5837(4)	1	2.10(2)	0.0142(7)
O12	0.3285(3)	0.6801(4)	0.4989(5)	1	1.92(2)	0.0142(7)
O13	0.0061(4)	0.7539(4)	0.4395(5)	1	2.30(3)	0.0142(7)
O14	0.5057(4)	0.6795(4)	0.4242(5)	1	1.86(2)	0.0142(7)
O15	0.5957(3)	0.5714(3)	0.3256(6)	1	2.10(2)	0.0142(7)
O16	−0.0750(4)	0.6601(6)	0.2673(5)	1	2.18(4)	0.0142(7)
O17	0.5081(4)	0.5656(3)	0.9308(7)	1	1.97(4)	0.0142(7)
O18	0.4154(3)	0.5581(3)	0.2433(6)	1	1.80(3)	0.0142(7)
O19	0.2049(4)	0.7824(4)	0.6227(3)	1	1.97(2)	0.0142(7)
O20	0.2597(3)	0.8699(4)	0.8498(5)	1	2.17(5)	0.0142(7)
O21	0.6366(4)	0.7710(6)	0.3106(4)	1	1.98(3)	0.0142(7)
O22	0.3458(2)	0.8364(4)	0.5051(5)	1	1.83(2)	0.0142(7)
O23	0.4324(3)	0.5751(3)	0.6649(6)	1	1.84(2)	0.0142(7)
O24	0.2411(3)	0.8484(3)	0.1059(5)	1	1.83(2)	0.0142(7)
O25	0.4173(4)	0.8390(5)	0.1547(5)	1	2.06(4)	0.0142(7)
O26	0.3528(3)	0.6873(3)	0.7662(5)	1	2.18(3)	0.0142(7)
O27	0.4922(2)	0.8233(9)	0.4162(6)	1	2.07(3)	0.0142(7)
O28	0.0120(4)	0.7765(5)	0.1738(6)	1	1.93(3)	0.0142(7)
O29	0.3297(3)	0.7219(5)	0.2526(5)	1	1.87(3)	0.0142(7)
O30	0.3179(4)	0.7361(4)	0.9859(4)	1	2.15(2)	0.0142(7)
Ow1	0.0966(8)	0.4688(7)	0.0558(12)	0.79(2)	0.04(3)	0.05(1)
Ow2	0.7994(11)	0.5310(9)	0.1887(16)	0.56(2)	0.30(1)	0.05(1)
Ow3	0.5141(11)	0.9703(8)	0.223(3)	0.33(2)	0.03(2)	0.05(1)
Ow4	0.3202(7)	0.9860(4)	0.0935(7)	0.53(2)	0.50(2)	0.05(1)
H1o1	0.1921(17)	0.594(4)	0.0319(10)	1	1.01(3)	0.01704
H1o2	0.2792(6)	0.598(2)	0.942(2)	1	1.01(3)	0.01704
H2o2	0.3376(10)	0.573(4)	0.0838(12)	1	1.05(3)	0.01704
H1o3	0.6027(17)	0.849(2)	0.0080(10)	1	1.08(4)	0.01704
H2o3	0.6555(9)	0.8725(16)	0.1413(18)	1	1.01(3)	0.01704
H1o6	0.1661(18)	0.9654(6)	0.500(4)	1	0.98(4)	0.01704
H1o7	0.232(2)	0.5334(17)	0.555(3)	1	0.95(6)	0.01704
H1o9	0.6416(5)	0.5383(12)	0.680(3)	1	0.95(4)	0.01704
H2o9	0.5438(7)	0.5529(10)	0.659(3)	1	1.06(4)	0.01704
H1o10	0.2064(11)	0.5427(10)	0.2688(13)	1	0.95(4)	0.01704
H2o10	0.3037(9)	0.5663(15)	0.248(4)	1	1.04(4)	0.01704
H1o15	0.6103(9)	0.5171(3)	0.334(4)	1	1.05(2)	0.01704
H1o16	−0.0909(18)	0.670(3)	0.1706(9)	1	1.05(3)	0.01704
H1o17	0.5710(6)	0.566(4)	0.923(3)	1	1.01(3)	0.01704
H2o17	0.4688(9)	0.5513(15)	0.8445(8)	1	1.02(2)	0.01704
H1o20	0.2328(4)	0.9199(5)	0.857(3)	1	0.99(2)	0.01704
H2o20	0.3009(11)	0.8736(17)	0.7898(19)	1	1.01(4)	0.01704
H1o25	0.445(2)	0.8196(11)	0.2444(9)	1	1.05(3)	0.01704

* Isotropic displacement parameters are from the kinematical refinement. [#] – bond-valence parameters are taken from Gagné and Hawthorne (2015)

Tab. 5 Selected interatomic distances (in Å) and angles (°) in the structure of krupičkaite

O–H (OH)		Cu–O		As–O	
O1–H1O1	0.982(14)	Cu1–O2	1.968(8)	As1–O4	1.664(6)
O6–H1O6	0.983(19)	Cu1–O8	2.023(5)	As1–O6	1.729(7)
O7–H1O7	0.98(3)	Cu1–O13	2.027(8)	As1–O19	1.679(6)
O15–H1O15	0.980(9)	Cu1–O17	2.230(7)	As1–O22	1.680(4)
O16–H1O16	0.981(13)	Cu1–O26	2.113(5)	As2–O1	1.708(8)
O25–H1O25	0.980(14)	Cu1–O30	2.093(7)	As2–O11	1.659(6)
O–H (H₂O)		Cu2–O4	2.273(5)	As2–O21	1.683(8)
O2–H1O2	0.980(17)	Cu2–O9	1.977(8)	As2–O27	1.667(4)
O2–H2O2	0.981(17)	Cu2–O11	1.960(9)	As3–O5	1.675(7)
O3–H1O3	0.98(2)	Cu2–O14	2.376(5)	As3–O13	1.632(5)
O3–H2O3	0.980(15)	Cu2–O24	2.004(5)	As3–O16	1.699(8)
O9–H1O9	0.98(2)	Cu2–O28	1.937(7)	As3–O28	1.676(7)
O9–H2O9	0.98(2)	Cu3–O19	1.911(4)	As4–O24	1.640(6)
O10–H1O10	0.98(2)	Cu3–O20	1.957(8)	As4–O25	1.724(7)
O10–H2O10	0.983(17)	Cu3–O21	2.157(7)	As4–O29	1.681(7)
O17–H1O17	0.981(15)	Cu3–O26	1.922(7)	As4–O30	1.661(5)
O17–H2O17	0.980(12)	Cu3–O30	1.921(5)	As5–O7	1.705(6)
O20–H1O20	0.980(11)	Cu4–O12	1.955(7)	As5–O12	1.672(6)
O20–H2O20	0.98(2)	Cu4–O14	1.936(7)	As5–O23	1.639(5)
angle H1Oᵢ–Oᵢ–H2Oᵢ [°]		Cu4–O22	1.975(7)	As5–O26	1.651(6)
O2	108(2)	Cu4–O27	1.833(12)	As6–O8	1.641(7)
O3	98(2)	Cu4–O28	2.336(6)	As6–O14	1.697(6)
O9	98(2)	Cu4–O29	2.341(5)	As6–O15	1.716(5)
O10	109(2)	Cu5–O3	1.769(11)	As6–O18	1.649(6)
O17	109(2)	Cu5–O8	2.015(9)		
O20	109(2)	Cu5–O13	1.953(4)		
		Cu5–O19	2.342(7)		
		Cu5–O21	1.961(5)		
		Cu6–O4	1.969(8)		
		Cu6–O5	1.984(7)		
		Cu6–O10	1.963(8)		
		Cu6–O11	2.220(5)		
		Cu6–O12	2.366(5)		
		Cu6–O29	1.981(6)		

distance between two copper-arsenate layers varies from 2.58 Å (like in geminite) to 5.92 Å, which results in channels running along **c** and occupied by molecular water (Figs 4b and 5).

7.2. Structural formula

The bond valence analysis, as well as the refinement of 3D ED data, gives an average composition of $Cu_6(H_2O)_6[AsO_3(OH)]_6$ with about 2.2 additional H_2O in the channel (Tab. 5). This result is consistent with the formula obtained after the chemical analyses of krupičkaite by electron microprobe. The latest analysis allowed the detection of a non-negligible amount of Co, Ni and Zn sharing the copper sites. In theory, the amount of water intra-channel can range from 0 to 4 when all water oxygen sites are either empty or fully occupied, leading to theoretical compositions from $Cu_6[AsO_3(OH)]_6·6H_2O$ to $Cu_6[AsO_3(OH)]_6·10H_2O$. On average, krupičkaite possesses $8H_2O$ (with 2 intra-channel H_2O). The likely local variation of the water content in the channel within one crystal

Cu atoms that are linked by vertices with AsO_4 tetrahedra along [–101]. The As-tetrahedra ensure the link between the Cu chain within one layer by three of their vertices, while the last one is staggered towards the interlayer and corresponds to the acid group. This group is further involved in hydrogen bonding and, thus, the layers' cohesion following the stacking direction. The layered structure of krupičkaite presents the alternation of $[Cu(AsO_3(OH))(H_2O)]^0$ sheets and an interlayer of molecular H_2O stacked along **b** (Figs 4c and 5). The

of krupičkaite may result in a stretching/shrinking of the channel's height along **b.** The stacking disorder in krupičkaite is then easily explained by the possible cleavage between the two kinds of sheets linked by strong hydrogen bonds and the likely flexibility of the intra-channel H_2O content and the H_2O connectivity. In this way, krupičkaite tend to behave like a 2D structure. The vast diversity of O–H···H bonds present in this mineral is supported by the Raman spectroscopy.

Tab. 6 Overview of related layered cooper-arsenate minerals

| Mineral	Composition	As/Cu (overall)	As/Cu (As–Cu layer)	As–Cu (layer)	Interlayer
Krupičkaite	$Cu_6[AsO_3(OH)]_6·8H_2O$	1	1	Chain 1: $CuΦ_5$ and $CuΦ_6$; Chain 2: $CuΦ_6$	H_2O
Geminite	$Cu(AsO_3OH)·H_2O$	1	1	Layer 1: $CuΦ_5$ and $CuΦ_6$; Layer2: $CuΦ_6$	H_2O
Slavkovite	$Cu_{13}(AsO_4)_6(AsO_3OH)_4·23H_2O$	1.3	1.1	$CuΦ_5$ and $CuΦ_6$	$CuΦ_4$ and H_2O
Ondrušite	$CaCu_4(AsO4)_2(AsO_3OH)_2·10H_2O$	1	1	$CuΦ_5$ and $CuΦ_6$	$CaΦ_6$ and H_2O
Lindackerite	$CuCu_4(AsO4)_2(AsO_3OH)_2·9H_2O$	1.25	1	$CuΦ_5$ and $CuΦ_6$	$CuΦ_6$ and H_2O
Yvonite	$Cu[AsO_3(OH)]·2H_2O$	1	1	$CuΦ_4$	H_2O
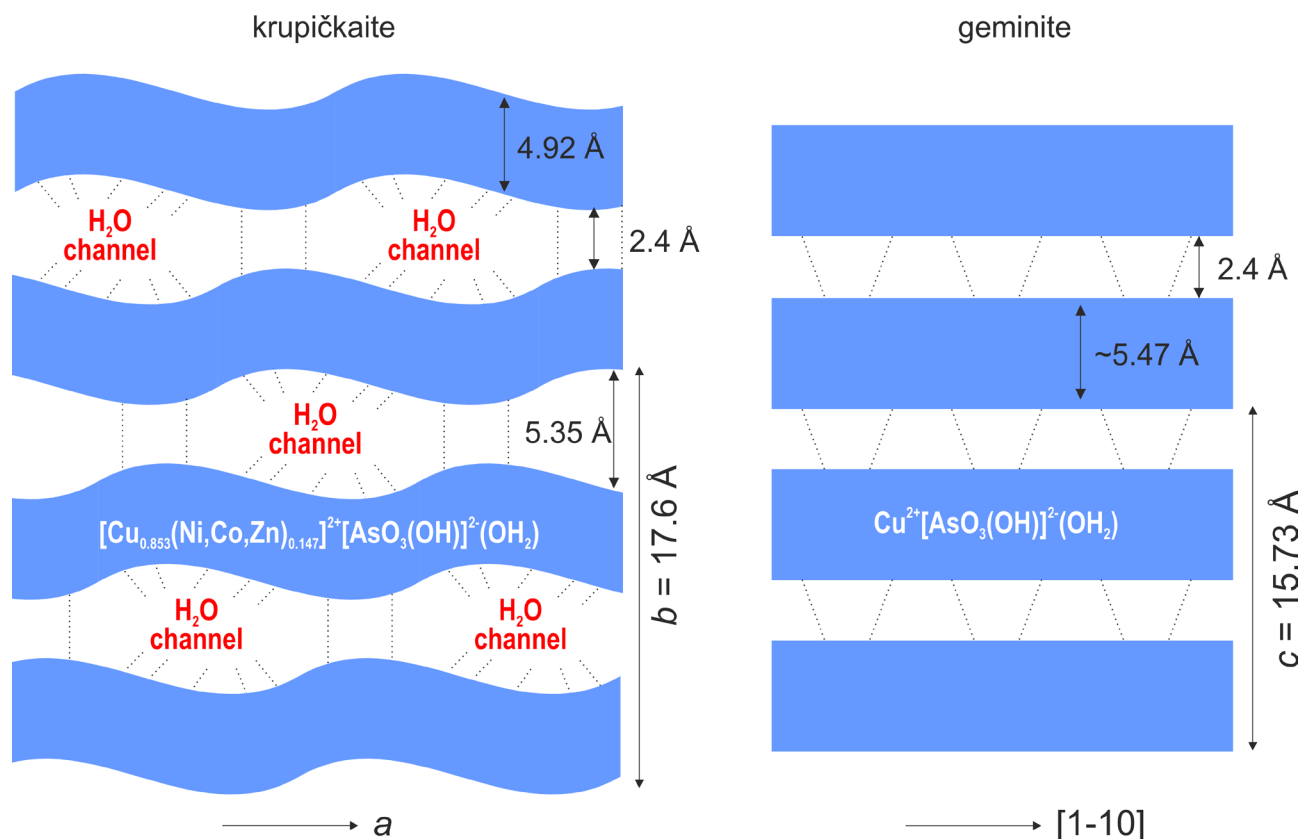
Fig. 5 Schemes of the stacking for krupičkaite (left) and geminite. The dashed lines represent O–H···O bonds and the O–H as well as hydrogen–bonds.

7.3. Comparison with related minerals

Considering the composition, the cation coordination, as well as the topology, the structure of krupičkaite is closely related to geminite, $Cu(AsO_3OH) \cdot H_2O$. At first sight and from the composition, one could consider krupičkaite to be a hydrated geminite with an additional 2/3 H_2O (Figs 4d and 5). However, a closer look at the topology of the two minerals reveals essential differences. In geminite, the Cu chains are linked the same way as in krupičkaite, but there are two different layers along the stacking direction **c** instead of one in krupičkaite: one with all the copper in octahedral coordination and the other presenting both octahedral and square pyramidal coordinations (Fig. 4d). Furthermore, the hydroxyl groups (acid groups) and the H_2O linked to As and Cu emanate out of the layers towards the next copper-arsenate layer, stabilizing the entire structure by hydrogen bonds (Fig. 5). In krupičkaite, the same feature is observed when two Cu-As layers are 2.58 Å away, while in the channels, the hydrogen bonds occur between the hydroxyl or the water molecules of the copper-arsenate layer and/or the surrounding water of the channel. The partial presence of water in the channel implies that the copper-arsenate layers are not linked by strong hydrogen bonds on all their surface, explaining well the easy cleavage observed in krupičkaite.

More generally, krupičkaite is related to several other layered copper arsenate minerals initially found in the Jáchymov ore district. Some of them possess the same, or close, As/Cu ratio of the As-Cu layers such as slavkovite (Sejkora et al. 2010c), other minerals of the lindackerite supergroup (Sejkora et al. 2011; Plášil et al. 2014a, b), or yvonite (Sarp and Černý 1998) among others (Tab. 6). Interestingly, except for yvonite that is built from infinite layers of $Cu\Phi_4$ linked with AsO_4 tetrahedra, other minerals present very characteristically collapsed copper chains in the arsenate-copper sheets. In krupičkaite, only one As-Cu layer is present but with two distinct chains, whereas, in slavkovite and minerals of the lindackerite supergroup, the main copper-arsenate layer is built upon chains with a mix of $Cu\Phi_5$ and $Cu\Phi_6$ polyhedra similarly bonded through AsO_4 tetrahedra. Slavkovite is another example of a highly hydrated mineral with a very thick water interlayer that seems to adopt a somewhat wavy arsenate copper sheet like in krupičkaite.

References

BORČINOVÁ RADKOVÁ A, JAMIESON H, LALINSKÁ-VOLEKOVÁ B, MAJZLAN J, ŠTEVKO M, CHOVAN M (2017) Mineralogical controls on antimony and arsenic mobility during tetrahedrite–tennantite weathering at historic mine sites Špania Dolina-Piesky and Ľubietová-Svätodušná, Slovakia. Amer Miner 102: 1091–1100

BRÁZDA P, PALATINUS L, DRAHOKOUPIL J, KNÍŽEK K, BURŠÍK J (2016) Calcium-induced cation ordering and large resistivity decrease in $Pr_{0.3}CoO_2$. J Phys Chem Solids 96–97: 10–16

BURNHAM CW (1962) Lattice constant refinement. Carnegie Institute Washington Yearbook 61: 132–135

BURNS PC, HAWTHORNE FC (1995) Coordination geometry structural pathways in Cu^{2+} oxysalt minerals. Canad Mineral 33: 889–905

ČEJKA J, SEJKORA J, BAHFENNE S, PALMER SJ, PLÁŠIL J, FROST RL (2011) Raman spectroscopy of hydrogen-arsenate group (AsO_3OH) in solid-state compounds: cobalt mineral phase burgessite $Co_2(H_2O)_4[AsO_3OH]_2 \cdot H_2O$. J Raman Spec 42: 214–218

CHRISTY AG (2015) Causes of anomalous mineralogical diversity in the periodic table. Mineral Mag 79: 33–49

CLABBERS M, GRUENE T, VAN GENDEREN E, ABRAHAMS JP (2019) Reducing dynamical electron scattering reveals hydrogen atoms. Acta Crystallogr A75: 82–93

COOPER MA, HAWTHORNE FC (1995) The crystal structure of geminite, $Cu^{2+}(AsO_3OH)(H_2O)$, a heteropolyhedral sheet structure. Canad Mineral 33: 1111–1118

ĐORĐEVIĆ T, KOLITSCH U, SERAFIMOVSKI T, TASEV G, TEPE N, STÖGER-POLLACH M, HOFMANN T, BOEV B (2019) Mineralogy and weathering of realgar-rich tailings at a former As-Sb-Cr mine at Lojane, North Macedonia. Canad Mineral 57: 403–423

GAGNÉ OC, HAWTHORNE FC (2015) Comprehensive derivation of bond-valence parameters for ion pairs involving oxygen. Acta Crystallogr B71: 562–578

GEMMI M, LANZA AE (2019) 3D electron diffraction techniques. Acta Crystallogr B 75: 495–504

GEMMI M, MUGNAIOLI E, GORELIK TE, KOLB U, PALATINUS L, BOULLAY P, HOVMÖLLER S, ABRAHAMS JP (2019) 3D Electron Diffraction: The Nanocrystallography Revolution. ACS Cent Sci 5: 1315–1329

HLOUŠEK J, PLÁŠIL J, SEJKORA J, ŠKÁCHA P (2014) News and new minerals from Jáchymov, Czech Republic (2003–2014). Bull mineral-petrolog Odd Nár Muz (Praha) 22: 155–181 (in Czech)

HORÁK V, ŠKÁCHA P, PLÁŠIL J (2014) History of mining on the Geister vein in the western part of the Jáchymov ore district. Bull mineral-petrolog Odd Nár Muz (Praha) 22: 192–192 (in Czech)

KEIM MF, STAUDE M, MARQUARDT K, BACHMANN K, OPITZ J, MARKL G (2018) Weathering of Bi-tennantite. Chem Geol 499: 1–25

KOLB U, GORELIK T, KUBEL C, OTTEN MT, HUBERT V (2007) Towards automated diffraction tomography: Part I – Data acquisition. Ultramicroscopy 107: 507–513

KOLB U, GORELIK T, KUBEL C, OTTEN MT (2008) Towards automated diffraction tomography. Part II – Cell parameter determination. Ultramicroscopy 108: 763–772

KRYSIAK Y, BARTON B, MARLER B, NEDER RB, KOLB U (2018) Ab initio structure determination and quantitative disorder analysis on nanoparticles by electron diffraction tomography. Acta Crystallogr A74: 93–101

LATYCHEVSKAIA T, ABRAHAMS JP (2019) Inelastic scattering and solvent scattering reduce dynamical diffraction in biological crystals. Acta Crystallogr B75: 523–531

MAJZLAN J, DRAHOTA P, FILIPPI M (2014) Parageneses and crystal chemistry of As minerals. Rev Mineral Geochem 79: 17–184

MAJZLAN J, KIEFER S, HERRMANN J, ŠTEVKO M, SEJKORA J, CHOVAN M, LÁNCZOS T, LAZAROV M, GERDES A, LANGENHORST F, BORČINOVÁ RADKOVÁ A, JAMIESON H, MILOVSKÝ R (2018) Synergies in elemental mobility during weathering of tetrahedrite $[(Cu,Fe,Zn)_{12}(Sb,As)_4S_{13}]$: Field observations, electron microscopy, isotopes of Cu, C, O, radiometric dating, and water geochemistry. Chem Geol 48: 1–20

MAJZLAN J, PLÁŠIL J, DACHS E, BENISEK A, MANGOLD S, ŠKODA R, ABROSIMOVA N (2021) Prediction and observation of formation of Ca-Mg arsenates in acidic and alkaline fluids: Thermodynamic properties and mineral assemblages at Jáchymov, Czech Republic and Rotgülden, Austria. Chem Geol 559: 119922

MUGNAIOLI E, GORELIK TE (2019) Structure analysis of materials at the order-disorder borderline using three-dimensional electron diffraction. Acta Crystallogr B75: 550–563

MUGNAIOLI E, GORELIK T, KOLB U (2009) "Ab-initio" structure solution from electron diffraction data obtained by a combination of automated diffraction tomography and precession technique. Ultramicroscopy 109: 758–765

MUGNAIOLI E, LANZA AE, BORTOLOZZI G, RIGHI L, MERLINI M, CAPPELLO V, MARINI L, ATHANASSIOU A, GEMMI M (2020) Electron Diffraction on Flash-Frozen Cowle-

site Reveals the Structure of the First Two-Dimensional Natural Zeolite. ACS Cent Sci 6, 9: 1578–1586

NEAGU A, TAI CW (2017) Local disorder in $Na_{0.5}Bi_{0.5}TiO_3$ – piezoceramic determined by 3D electron diffuse scattering. Sci Rep 7: 1–12

ONDRUŠ P (1993) A computer program for analysis of X-ray powder diffraction patterns. Materials Science Forum, EPDIC–2, Enchede, 133–136, 297–300

ONDRUŠ P, VESELOVSKÝ F, GABAŠOVÁ A, HLOUŠEK J, ŠREIN V (2003) Geology and hydrothermal vein system of the Jáchymov (Joachimsthal) ore district. J Czech Geol Soc 48: 3–18

PALATINUS L, CHAPUIS G (2007) Superflip – a computer program for the solution of crystal structures by charge flipping in arbitrary dimensions. J Appl Cryst 40: 451–456

PALATINUS L, PETŘÍČEK V, CORRÊA CA (2015a) Structure refinement using precession electron diffraction tomography and dynamical diffraction: theory and implementation. Acta Crystallogr A71: 235–24

PALATINUS L, CORRÊA CA, STECIUK G, JACOB D, ROUSSEL P, BOULLAY P, KLEMENTOVÁ M, GEMMI M, KOPEČEK J, DOMENEGHETTI MCH, CÁMARA F, PETŘÍČEK V (2015b) Structure refinement using precession electron diffraction tomography and dynamical diffraction: tests on experimental data. Acta Crystallogr B71: 740–751

PALATINUS L, BRÁZDA P, BOULLAY P, PEREZ O, KLEMENTOVÁ M, PETIT S, EIGNER V, ZAAROUR M, MINTOVA S (2017) Hydrogen positions in single nanocrystals revealed by electron diffraction. Science 355: 166–169

PALATINUS L, BRÁZDA P, JELÍNEK M, HRDÁ J, STECIUK G, KLEMENTOVÁ M (2019) Specifics of the data processing of precession electron diffraction tomography data and their implementation in the program PETS2.0. Acta Crystallogr B75: 512–522

PETŘÍČEK V, DUŠEK M, PALATINUS L (2014) Crystallographic Computing System Jana 2006: general features. Z Kristallogr 229: 345–352

PLÁŠIL J, SEJKORA J, ŠKODA R, NOVÁK M, KASATKIN AV, ŠKÁCHA P, VESELOVSKÝ F, FEJFAROVÁ K, ONDRUŠ P (2014a) Hloušekite, $(Ni,Co)Cu_4(AsO_4)_2(AsO_3OH)_2(H_2O)_9$, a new member of the lindackerite supergroup from Jáchymov, Czech Republic. Mineral Mag 78: 1341–1353

PLÁŠIL J, KASATKIN AV, ŠKODA R, ŠKÁCHA P (2014b) Klajite, $MnCu_4(AsO_4)_2(AsO_3OH)_2(H_2O)_{10}$, from Jáchymov (Czech Republic): the second world occurrence. Mineral Mag 78: 134–143

PLÁŠIL J, ŠKÁCHA P, SEJKORA J, ŠKODA R, NOVÁK M, VESELOVSKÝ F, HLOUŠEK J (2017) Babánekite, $Cu_3(AsO_4)_2\cdot8H_2O$, from Jáchymov, Czech Republic – a new member of the vivianite group. J Geosci 62: 261–270

POUCHOU JL, PICHOIR F (1985) "PAP" ($\varphi\rho Z$) procedure for improved quantitative microanalysis. In: ARMSTRONG J T (ed) Microbeam Analysis. San Francisco Press, San Francisco, 104–106

PRENCIPE M, PUSHCHAROVSKII DYU, SAROM H, FERRARIS D (1996) Comparative crystal chemistry of geminite $Cu(AsO_3OH)\cdot(H_2O)$ and minerals related to it. Vestnik Moskovskogo Universiteta, Seriya 4: Geologiya 4: 66–74

SARP H, ČERNÝ R (1998) Description and crystal structure of yvonite. Amer Miner 83: 383–389

SEJKORA J, PLÁŠIL J, VESELOVSKÝ F, CÍSAŘOVÁ I, HLOUŠEK J (2011) Ondrušite, $CaCu_4(AsO_4)_2(AsO_3OH)_2\cdot10H_2O$, a new mineral species from the Jáchymov ore district, Czech Republic: Description and crystal-structure determination. Canad Mineral 49: 885–897

SEJKORA J, PLÁŠIL J, ONDRUŠ P, VESELOVSKÝ F, CÍSAŘOVÁ I, HLOUŠEK J (2010c) Slavkovite, $Cu_{13}(AsO_4)_6(AsO_3OH)_4\cdot23H_2O$, a new mineral species from Horní Slavkov and Jáchymov, Czech Republic: description and crystal-structure determination. Canad Mineral 48: 1157–1170

SEJKORA J, ČEJKA J, FROST RL, BAHFENNE S, PLÁŠIL J, KEEFFE EC (2010b) Raman spectroscopy of hydrogen-arsenate group (AsO_3OH) in solid-state compounds: copper mineral phase geminite $Cu(AsO_3OH)\cdot H_2O$ from different geological environments. J Raman Spectrosc 41: 1038–1043

SEJKORA J, ONDRUŠ P, NOVÁK M (2010a) Veselovskýite, triclinic $(Zn,Cu,Co)Cu_4(AsO_4)_2(AsO_3OH)_2\cdot9H_2O$, a Zn-dominant analogue of lindackerite. N Jb Mineral Abh 187: 83–90

SEJKORA J, PLÁŠIL J, ČEJKA J, DOLNÍČEK Z, PAVLÍČEK R (2020) Molecular structure of the arsenate mineral chongite from Jáchymov – a vibrational spectroscopy study. J Geosci 65: 111–120

ŠKÁCHA P, PLÁŠIL J, HORÁK V (2019) Jáchymov – mineralogická perla Krušnohoří. Academia, Praha, pp 1–688

STECIUK G, GHAZISAEED S, KIEFER B, PLÁŠIL J (2019a) Crystal structure of vyacheslavite, $U(PO_4)(OH)$, solved from natural nanocrystal: a precession electron diffraction tomography (PEDT) study and DFT calculations. RSC Adv 9: 19657

STECIUK G, PALATINUS L, ROHLÍČEK J, OUHENIA S, CHATEIGNER D (2019b) Stacking sequence variations in vaterite resolved by precession electron diffraction tomography using a unified superspace model. Sci Rep 9: 1–12

STECIUK G, ŠKODA R, ROHLÍČEK J, PLÁŠIL J (2020) Crystal structure of the uranyl-molybdate mineral calcurmolite $Ca[(UO_2)_3(MoO_4)_2(OH)_4](H_2O)_{-5.0}$: insights from a precession electron-diffraction tomography study. J Geosci 65: 15–25

STECIUK G, MAJZLAN J, PLÁŠIL J (2021) Hydrogen disorder in kaatialaite $Fe[AsO_2(OH)_2]5H_2O$ from Jáchymov, Czech Republic: determination from low-temperature 3D electron diffraction. IUCr Journal 8: 2052–2525

VANSANT FK, VAN DER VEKEN BJ, DESSEYN HD (1973) Vibrational analysis of arsenic and its anions I. Description of the Raman spectra. J Mol Struct 15: 425–437

Vincent R, Midgley PA (1994) Double conical beam–rocking system for measurement of integrated electron diffraction intensities. Ultramicroscopy 53: 271–282

Zhao H, Krysiak Y, Hoffmann K, Barton B, Molina-Luna L, Neder RB, Kleebe HJ, Gesing TM, Schneider H, Fischer RX, Kolb U (2017) Elucidating structural order and disorder phenomena in mullite-type $Al_4B_2O_9$ by automated electron diffraction tomography. J Solid State Chem 249: 114–123